NANO LETTERS

Letter

pubs.acs.org/NanoLett

New Insight in Understanding Oxygen Reduction and Evolution in Solid-State Lithium–Oxygen Batteries Using an in Situ Environmental Scanning Electron Microscope

Hao Zheng,[†] Dongdong Xiao,[†] Xing Li,[‡] Yali Liu,[†] Yang Wu,[§] Jiaping Wang,[§] Kaili Jiang,[§] Chun Chen,[∥] Lin Gu,*[,†] Xianlong Wei,*[,‡] Yong-Sheng Hu,*[,†] Qing Chen,[‡] and Hong Li[†]

[†]Beijing National Laboratory for Condensed Matter Physics, Institute of Physics, Chinese Academy of Sciences, Beijing, 100190, P. R. China

[‡]Key Laboratory for the Physics and Chemistry of Nanodevices, Department of Electronics, Peking University, Beijing 100871, P. R. China

[§]Department of Physics and Tsinghua-Foxconn Nanotechnology Research Center, Tsinghua University, Beijing, P. R. China, 100084

[∥]Department of Chemistry, Beijing Institute of Technology, Beijing, P. R. China, 102488

Supporting Information

ABSTRACT: Via designing a facile microscale all-solid-state lithium–oxygen battery system constructed in an environmental scanning electron microscope, direct visualization of discharge and charge processes of the lithium–oxygen battery is achieved. Different morphologies of the discharge product are observed, including a sphere, conformal film, and red-blood-cell-like shape, with a particle size up to 1.5 μm; whereas upon charge, the decomposition initiates at their surface and continues along a certain direction, instead of from the contact point at the electrode. These new findings indicate that the electron and lithium ion conductivities of Li_2O_2 could support the growth and decomposition of the discharge product in our system. In addition, our results indicate that various morphologies of Li_2O_2 arise from the different current density and surface chemistry of CNT, and the growth and decomposition of the particle are related to the uneven distribution of the ionic and electronic conductivities of Li_2O_2.

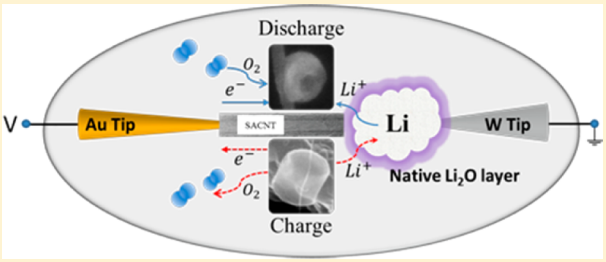

KEYWORDS: *Lithium–oxygen battery, in situ ESEM, lithium peroxide, decomposition, electron transport*

The rechargeable nonaqueous lithium–oxygen ($Li–O_2$) battery has attracted worldwide attention recently due to its much higher theoretical energy density compared to current state-of-the-art lithium-ion batteries and has been considered as one of the promising candidates to meet the ever-increasing demand for high-energy storage in the electric vehicle field.[1−3] However, numerous challenges hinder its practical applications, including low round-trip efficiency, poor rate capability, and cycle life on the side of the oxygen electrode.[4,5]

Successfully addressing these challenges needs to elucidate the fundamental scientific problems involved in $Li–O_2$ batteries, such as the mechanism of oxygen reduction reaction (ORR) and oxygen evolution reaction (OER) and the kinetics of charge transport (ion transport and electron transport). Therefore, much effort has been directed toward understanding the electrochemical reaction of $Li–O_2$ batteries during discharge and charge,[6−9] and several works on designing the cathode have been conducted based on this fundamental knowledge.[10−12] Now, it has been well-established that the overall electrochemical reaction in nonaqueous $Li–O_2$ battery is the reduction of oxygen to form Li_2O_2 by combining with Li upon discharge and its subsequent decomposition to release oxygen and Li upon charge.[13−16] It follows that the formation and decomposition of Li_2O_2 play a critical role in determining the discharge capacity, reversibility, discharge–charge profiles, and rate capability of the $Li–O_2$ battery. Consequently, extensive studies have been conducted to track the nucleation, growth, morphological evolution of Li_2O_2 during discharge and its oxidation during charge through ex situ approaches.[17−21] The post-mortem analysis has provided important insights into the mechanism of formation and decomposition of Li_2O_2, and the detailed dynamic process of $Li–O_2$ electrochemical reaction remains elusive. In addition, various in situ spectroscopy and/or diffraction techniques, such as ambient pressure X-ray photoelectron spectroscopy (XPS),[15] X-ray diffraction (XRD),[22] and surface enhanced Raman spectroscopy (SERS),[13] have also been adopted. However, these methods are incapable of directly following the growth, morphology, evolution, and disappearance of Li_2O_2. By virtue of in situ TEM, Zhong et al.

Received: March 6, 2014
Revised: June 25, 2014
Published: June 30, 2014

   dx.doi.org/10.1021/nl500862u | *Nano Lett.* 2014, 14, 4245−4249

observed the electrochemical oxidation of Li_2O_2, and concluded that electron transport in Li_2O_2 limited the oxidation kinetics.[23] But it should be noted that in their work the investigated Li_2O_2 particles were formed in an ether-based cell, before loading them onto the TEM sample holder, leading to possible contamination during microbattery construction and transfer. Only the decomposition of Li_2O_2 was studied during charge process, there remains lack of in situ visualization of growth and morphology of Li_2O_2.

To this end, we performed an in situ study on the discharge and charge processes of a microscale all-solid-state Li−O_2 battery built in an environmental scanning electron microscope (ESEM, FEI Quanta 600F), which was equipped with a nanoprobe system (Kleindiek). Unlike Zhong's work,[23] in this study, the entire experiment was conducted in situ without air exposure, and both discharge and charge processes were examined. Furthermore, our all-solid-state Li−O_2 battery also eliminates the undesirable decomposition reactions induced by the instability of liquid electrolytes at the attacks from reduced oxygen species (such as superoxide radical anion, Li_2O_2) during the discharge process and at a high oxidizing potential during the charge process. In addition, the irradiation effect in TEM is much stronger than that in SEM, which may complicate the interpretation of experimental data.

As shown in Figure 1, the microscale battery is constructed with the Li metal, the native oxide layer Li_2O,[24] and the super

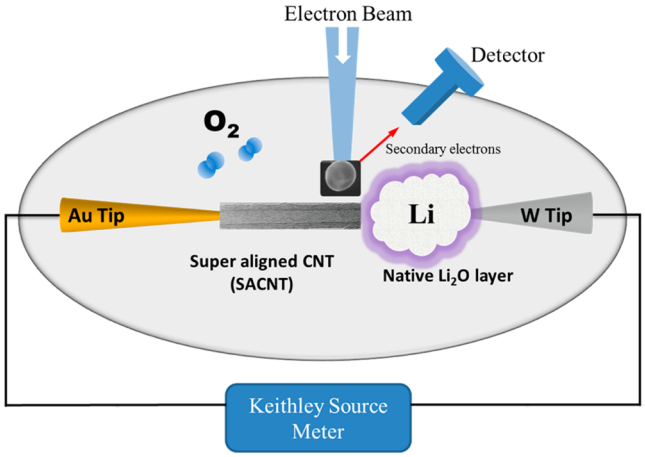

Figure 1. A schematic view of microscale all-solid-state Li−O_2 battery assembled in the ESEM chamber. The SACNT and lithium metal worked as the cathode and anode, respectively. The native oxide layer Li_2O on Li metal worked as the solid state electrolyte. The voltage was applied by Keithley 4200-SCS.

aligned carbon nanotube (SACNT)[25] as the anode, solid state electrolyte, and cathode, respectively. With the aid of the in situ technique in the ESEM, we first report the direct observation of formation of Li_2O_2 during discharge and its subsequent decomposition during charge, thereby providing important implications for understanding the kinetics of oxygen reaction and charge transport.

The discharge process of Li−O_2 battery was conducted under potentiostatic conditions. A bias of −3 V was applied on the SACNT vs Li metal to initiate the discharge process with the O_2 partial pressure being 200 Pa. Figure 2 shows product morphologies observed after discharge process, including a sphere and toroid or a red-blood-cell-like shape, which are in agreement with previous works based on the nonaqueous Li−

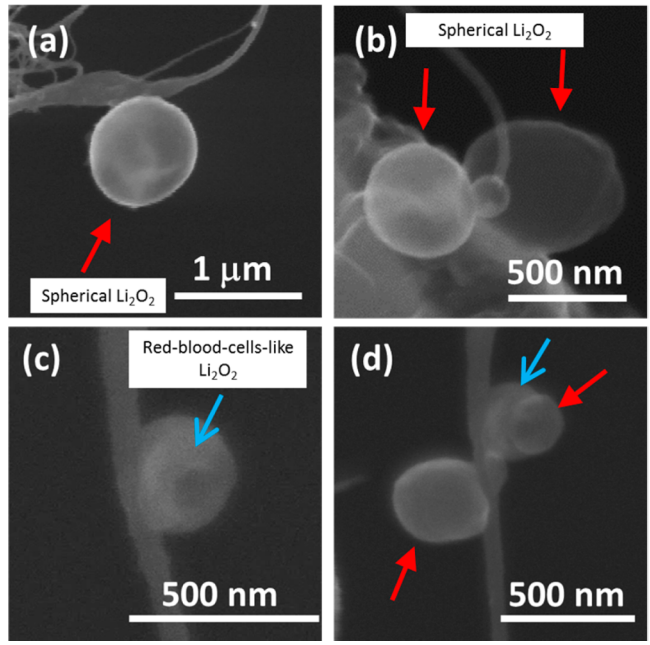

Figure 2. Product morphology observed during the discharge process, including spheres (parts a, b, d, indicated by the red arrow) and red-blood-cell-like particles (parts c, d, indicated by the blue arrow). Note that parts c and d demonstrate the same site of the CNT at different discharge states. In part c, the inner part of the particle is darker than the outer part; in part d, a new smaller particle grew up right upon the inner part of the same particle in part c.

O_2 battery containing relative stable electrolytes (e.g., ethers and DMSO).[26−29]

In addition, we conducted a comparative experiment under different conditions, i.e., with and without oxygen, as shown in Figure S4 in the Supporting Information, to further demonstrate that our all-solid-state battery undergoes an oxygen reduction reaction during discharge process. There is a major difference that under vacuum conditions the discharge product is dendrite-like, while under oxygen conditions, the discharge product turns into sphere-like or red-blood-cell-like particles. These characteristic morphologies, especially the red-blood-cell-like particles, suggest that these discharge products are mainly Li_2O_2.[30]

According to our experimental results as shown in Figure 2, some discharge products with particle sizes ranging from 500 nm to 1 μm tend to grow on the CNT−solid state electrolyte−oxygen three-phase interface (TPI) (as indicated by red arrows in Figure 2a,c), while some smaller discharge products tend to grow along the CNT away from the TPI (Figure 2c,d). Note that Figure 2a was captured after the lithium anode was detached (see Figure S3). In addition, Figure 2c,d demonstrates the same position of the CNT at different discharge states, and the particles indicated by the blue arrow are the same. As shown in Figure 2c, the inner part of the particle is darker than the outer part; in Figure 2d, a new smaller particle grew up right upon the inner part of the same particle in Figure 2c, which indicates the inner part of the particle in Figure 2c has a concave surface, like the morphology of red blood cells. These two figures demonstrate that a new particle can be able to grow on the surface of the red-blood-cell-like particle and its size is already beyond the electron tunneling distance (~5 nm) of insulating Li_2O_2.[31] These results indicate that the electronic and

dx.doi.org/10.1021/nl500862u | Nano Lett. 2014, 14, 4245−4249

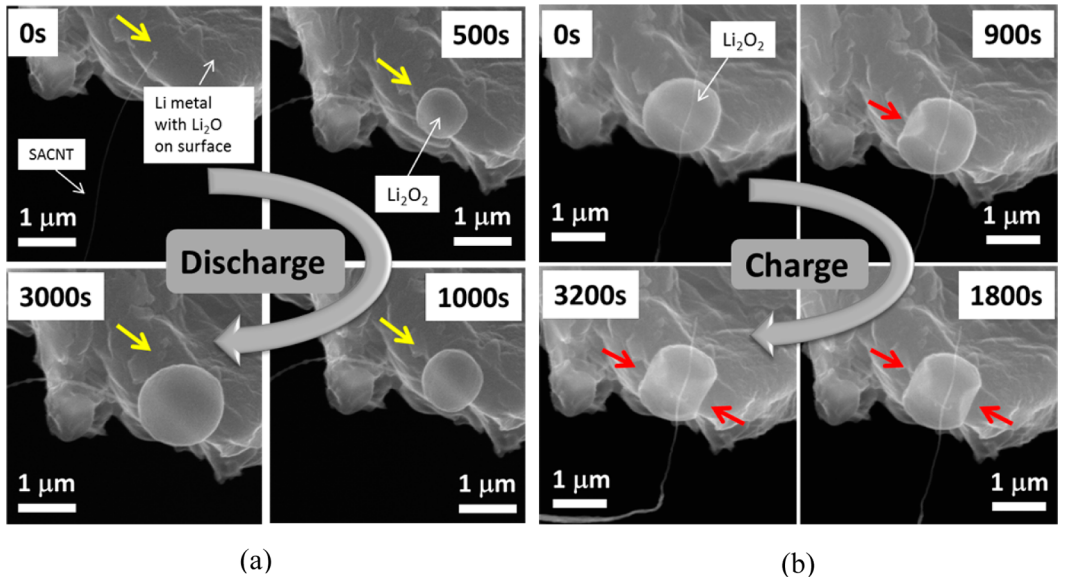

Figure 3. Discharge and charge processes of the Li−O_2 battery. (a) Images captured at 0, 500, 1000, and 3000 s show the growth process of a spherical particle, which can grow up to 1.5 μm. −3 V was applied on SACNT vs Li metal to initiate the discharge process. Yellow arrows indicate that the spherical particle grew up at a CNT−solid state electrolyte−oxygen TPI. Note that the CNT curved probably due to the sample drift. (b) Images captured at 0, 900, 1800, and 3200 s show the decomposition process of the spherical particle. 8 V was applied on SACNT vs Li metal to initiate the charge process. Red arrows indicate the position where the particle decomposed. Note that the electron beam was on only during the image acquisition to minimize the irradiation effect.

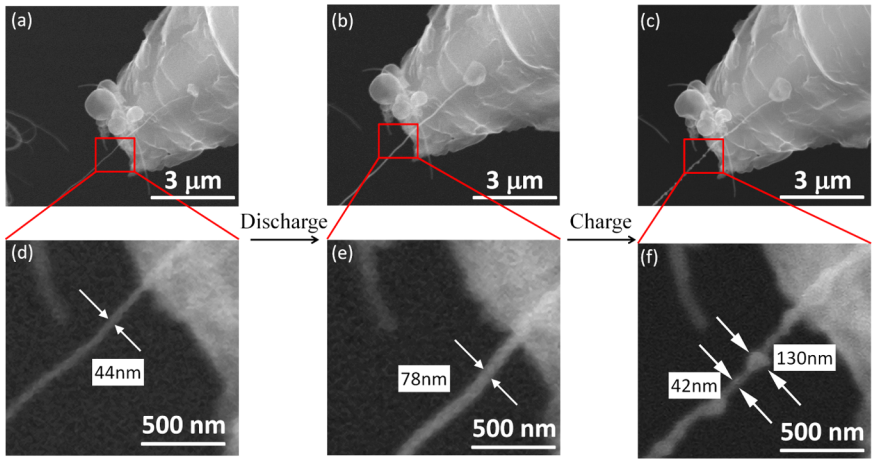

Figure 4. CNT morphology evolution during discharge and charge. Areas inside the red box in (a), (b), and (c) were enlarged in (d), (e), and (f), respectively. It indicates that the conformal film grown on the CNT decomposed to the beads during the charge process.

ionic conductivities of formed Li_2O_2 could support the growth of the discharge product.

Inspired by the above-mentioned results, an electrochemical cycle was conducted to follow the formation and decomposition of Li_2O_2 in the all-solid-state Li−O_2 battery. During discharge, a particle up to 1.5 μm appeared at the three-phase interface when the duration lasts for 3000 s (Figure 3a). Another fresh CNT was reconnected to the particle on the top when the charge process was performed with a voltage of 8 V applied to SACNT vs Li metal under vacuum conditions. Upon the charge process, the decomposition of the same particle initiated locally at the surface and proceeded into the bulk along a certain direction (Figure 3b), which was consistent with the observation by Jung and co-workers.[19] The large-sized particle observed in Figure 3 also indicates that the electronic and ionic conductivities of the particle are capable of supporting the particle's growth. According to the calculation results, the electronic conductivity on the surface of Li_2O_2 is higher than that in the bulk.[32] In addition, Gerbig et al. reported that measured ionic conductivity of Li_2O_2 is higher than its electronic conductivity at 100 °C.[33] Therefore, it is reasonable that the decomposition initiated from the particle's surface. Apart from the electronic and ionic transportation, the decomposition process may relate to or be limited by the oxygen transportation. According to the Le Chatelier's principle (the equilibrium law), the vacuum condition is beneficial for the charge process corresponding to $Li_2O_2 \rightarrow 2Li^+ + O_2 + 2e^-$. Thus, the decomposition occurred on the large bare surface area where it is favorable for the oxygen release caused by Li_2O_2 decomposition, rather than on the connect point of CNT−particle or particle−solid electrolyte. Note that in our experiments the electron beam was on only when the images were captured to minimize the irradiation effect.

dx.doi.org/10.1021/nl500862u | *Nano Lett.* 2014, 14, 4245−4249

In addition, it is worth noting that the diameter of SACNT increased from an initial 44 to 78 nm after discharge, expanding by 77% (Figure 4a,b,d,e), which is much larger than that of CNT induced by lithium insertion alone.[34] This indicates that a conformal film has grown along the CNT, the appearance of which may be related to the current density[21] and surface chemistry of CNT.[35] Another interesting phenomenon is that the bead morphology can be evolved from the conformal film during the decomposition process. By comparing the SEM image of the CNT cathode before and after the charge process (Figure 4b,c,e,f), the CNT becomes a little thinner after charge process, and it seems that the conformal film coated on the CNT decomposed to the beads during the charge process. Unexpectedly, the decomposition of Li_2O_2 is accompanied by the appearance of the beads. This may be caused by the conversion of Li_2O_2 to Li_2CO_3 with the presence of carbon or the resident gas in the vacuum chamber at a relative high potential.[36−38]

Taking more advantage of the ESEM in situ technique, we repeated the discharge and charge processes (i.e., cycle the in situ Li−O_2 battery); four discharge processes and three charge processes were recorded in video (see respective videos in the Supporting Information). Voltages of −3 and 6 V were applied on the SACNT vs Li metal to initiate the discharge and charge processes, respectively. This microscale all-solid-state Li−O_2 battery successfully cycled three times. During the third charge process (see video OER_3 in the Supporting Information), the conformal film began to decompose to beads along the SACNT, as was mentioned above, the conformal film may be oxidized to Li_2O or converted to Li_2CO_3 at a relative high potential and caused a poor electron transportation along the SACNT, which negatively affects the subsequent fourth discharge process (see video ORR_4 in the Supporting Information). Actually, the battery was still alive for a while at the beginning of fourth discharge process (the particle grew up a little). At 707 s, the beads along the SACNT became much bigger (Figure 5b), and the growth process ceased. These results imply that the side reaction of the carbon and discharge products could limit the battery cyclability. In addition, it is interesting to note that, during cycling, the growth and decomposition of the Li_2O_2 paritcle display inhomogeneity to some degree as shown in Figure S6 and S7 in the Supporting Information. Such an inhomogeneous process could be due to the uneven distribution of the electronic and ionic conductivities along the particle surfaces.

It should be noted that, in our battery configuration, the cathode is only in point contact with the electrolyte, while in a realistic nonaqueous Li−O_2 battery, the cathode is "immersed" in the electrolyte, which may cause the diffusion pattern of lithium ions modified.[38] However, some intrinsic phenomenon (e.g., electron and ion transportation in Li_2O_2) can be disclosed in such an open Li−O_2 cell. In addition, the characteristic red-blood-cell-like morphology is also observed in the all-solid-state Li−O_2 battery; it indicates that the formation of this morphology may relate to more intrinsic factors such as charge and mass transportation in Li_2O_2, and the epitaxial growth or deposition from nonaqueous electrolyte, as proposed in previous work,[16,18] may not be the exclusive way to form a red-blood-cell-like morphology.

In summary, we built an all-solid-state Li−O_2 battery based on an ESEM configuration and performed the both processes of discharge and charge of the battery in real-time. It is found that (i) the electronic and ionic conductivities of Li_2O_2 could be able to sustain the growth and decomposition of the discharge product; (ii) in our system, the decomposition process may relate to the kinetics of oxygen release. (iii) The bead-like by-product along SACNTs evolved from the Li_2O_2 conformal film could limit the battery cyclability; (iv) the growth and decomposition of Li_2O_2 are related to the uneven distribution of the ionic and electronic conductivities of the particle. These results present some new insights toward understanding the reaction mechanism of the all-solid-state Li−O_2 battery; further experiments under aprotic environments can be conducted, to approach working conditions of a real battery.

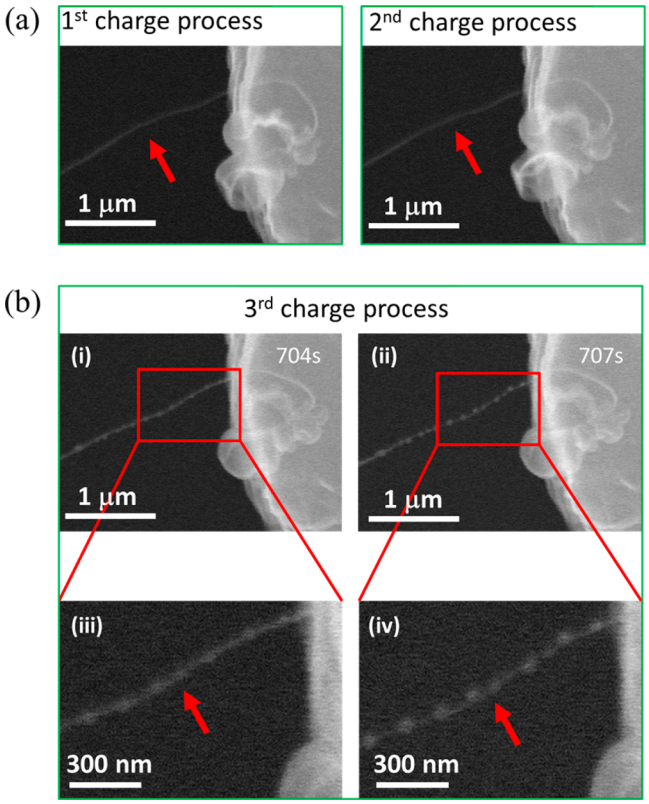

Figure 5. (a) SEM image at the end of the first (left) and second (right) charge processes wherein no beads are observed along the SACNT. (b) Image (i) and (ii) captured at 704 and 707 s upon the third charge process, respectively. Enlarged images (iii) and (iv) of the corresponding red box areas in (i) and (ii) show that the beads became larger at 707 s.

■ ASSOCIATED CONTENT

Supporting Information

Experimental details, photograph of experimental set-up, TEM images of the pristine CNT, and supplementary videos. This material is available free of charge via the Internet at http://pubs.acs.org.

■ AUTHOR INFORMATION

Corresponding Authors

*E-mail: l.gu@iphy.ac.cn (L.G.).
*E-mail: weixl@pku.edu.cn (X.L.W.).
*E-mail: yshu@iphy.ac.cn (Y.S.H.).

Author Contributions

H.Z., D.X., and X.L. contributed equally.

Notes

The authors declare no competing financial interest.

■ ACKNOWLEDGMENTS

The IOP group acknowledge the financial support from the "973" project (2014CB932300, 2012CB932900) and the NSFC (51325206, 51222210, 11174334). The PKU group is supported by NSFC (11374022, 61371001).

■ REFERENCES

(1) Abraham, K. M.; Jiang, Z. *J. Electrochem. Soc.* **1996**, *143*, 1−5.
(2) Ogasawara, T.; Débart, A.; Holzapfel, M.; Novák, P.; Bruce, P. G. *J. Am. Chem. Soc.* **2006**, *128*, 1390−1393.
(3) Bruce, P. G.; Freunberger, S. A.; Hardwick, L. J.; Tarascon, J. M. *Nat. Mater.* **2012**, *11*, 19−29.
(4) Girishkumar, G.; McCloskey, B.; Luntz, A. C.; Swanson, S.; Wilcke, W. *J. Phys. Chem. Lett.* **2010**, *1*, 2193−2203.
(5) Lu, Y. C.; Gallant, B. M.; Kwabi, D. G.; Harding, J. R.; Mitchell, R. R.; Whittingham, M. S.; Shao-Horn, Y. *Energy Environ. Sci.* **2013**, *6*, 750−768.
(6) Laoire, C. O.; Mukerjee, S.; Abraham, K. M.; Plichta, E. J.; Hendrickson, M. A. *J. Phys. Chem. C* **2009**, *113*, 20127−20134.
(7) Hassoun, J.; Croce, F.; Armand, M.; Scrosati, B. *Angew. Chem., Int. Ed.* **2011**, *50*, 2999−3002.
(8) Freunberger, S. A.; Chen, Y. H.; Peng, Z. Q.; Griffin, J. M.; Hardwick, L. J.; Bardé, F.; Novák, P.; Bruce, P. G. *J. Am. Chem. Soc.* **2011**, *133*, 8040−8047.
(9) Zhai, D. Y.; Wang, H. H.; Yang, J. B.; Lau, K. C.; Li, K.; Amine, K.; Curtiss, L. A. *J. Am. Chem. Soc.* **2013**, *135*, 15364−15372.
(10) Xiao, J.; Mei, D.; Li, X.; Xu, W.; Wang, D.; Graff, G. L.; Bennett, W. D.; Nie, Z.; Saraf, L. V.; Aksay, I. A.; Liu, J.; Zhang, J.-G. *Nano Lett.* **2011**, *11*, 5071−5078.
(11) Lim, H. D.; Park, K. Y.; Song, H.; Jang, E. Y.; Gwon, H.; Kim, J.; Kim, Y. H.; Lima, M. D.; Ovalle Robles, R.; Lepro, X.; Baughman, R. H.; Kang, K. *Adv. Mater.* **2013**, *25*, 1348−1352.
(12) Jian, Z.; Liu, P.; Li, F.; He, P.; Guo, X.; Chen, M.; Zhou, H. *Angew. Chem., Int. Ed.* **2014**, *53*, 442−446.
(13) Peng, Z. Q.; Freunberger, S. A.; Hardwick, L. J.; Chen, Y.; Giordani, V.; Bardé, F.; Novák, P.; Graham, D.; Tarascon, J. M.; Bruce, P. G. *Angew. Chem., Int. Ed.* **2011**, *50*, 6351−6355.
(14) McCloskey, B.; Scheffler, R.; Speidel, A.; Girishkumar, G.; Luntz, A. C. *J. Phys. Chem. C* **2012**, *116*, 23897−23905.
(15) Lu, Y. C.; Crumlin, E. J.; Veith, G. M.; Harading, J. R.; Mutoro, E.; Baggetto, L.; Dudney, N. J.; Liu, Z.; Shao-Horn, Y. *Sci. Rep.* **2012**, *2*, 715.
(16) Black, R.; Oh, S. H.; Lee, J. H.; Yim, T.; Adams, B.; Nazar, L. F. *J. Am. Chem. Soc.* **2012**, *134*, 2902−2905.
(17) Mitchell, R. R.; Gallant, B. M.; Thompson, C. V.; Shao-Horn, Y. *Energy Environ. Sci.* **2011**, *4*, 2952−2958.
(18) Mitchell, R. R.; Gallant, B. M.; Shao-Horn, Y.; Thompson, C. V. *J. Phys. Chem. Lett.* **2013**, *4*, 1060−1064.
(19) Jung, H. G.; Kim, H. S.; Park, J. B.; Oh, I. H.; Hassoun, J.; Yoon, C. S.; Scrosati, B.; Sun, Y. K. *Nano Lett.* **2012**, *12*, 4333−4335.
(20) Fan, W. G.; Cui, Z. H.; Guo, X. X. *J. Phys. Chem. C* **2013**, *117*, 2623−2627.
(21) Adams, B. D.; Radtke, C.; Black, R.; Trudeau, M. L.; Zaghib, K.; Nazar, L. F. *Energy Environ. Sci.* **2013**, *6*, 1772−1778.
(22) Lim, H.; Yilmaz, E.; Byon, H. R. *J. Phys. Chem. Lett.* **2012**, *3*, 3210−3215.
(23) Zhong, L.; Mitchell, R. R.; Liu, Y.; Gallant, B. M.; Thompson, C. V.; Huang, J. Y.; Mao, S. X.; Shao-Horn, Y. *Nano Lett.* **2013**, *13*, 2209−2214.
(24) Liu, X. H.; Huang, J. Y. *Energy Environ. Sci.* **2011**, *4*, 3844−3860.
(25) Wu, Y.; Wei, Y.; Wang, J.; Jiang, K.; Fan, S. *Nano Lett.* **2013**, *13*, 818−823.
(26) Yang, J.; Zhang, D.; Wang, H. H.; Lau, K. C.; Schlueter, J. A.; Du, P.; Myers, D. J.; Sun, Y. K.; Curtiss, L. A.; Amine, K. *Phys. Chem. Chem. Phys.* **2013**, *15*, 3764−3771.
(27) Xu, D.; Wang, Z. L.; Xu, J. J.; Zhang, L. L.; Zhang, X. B. *Chem. Commun.* **2012**, *48*, 6948−6950.
(28) Lim, H. D.; Park, K. Y.; Song, H.; Jang, E. Y.; Gwon, H.; Kim, J.; Kim, Y. H.; Lima, M. D.; Robles, R. O.; Lepro, X.; Baughman, R. H.; Kang, K. *Adv. Mater.* **2013**, *25*, 1348−1352.
(29) Xu, J. J.; Wang, Z. L.; Xu, D.; Zhang, L. L.; Zhang, X. B. *Nat. Commun.* **2013**, *4*, 2438.
(30) Lu, Y.-C.; Kwabi, D. G.; Yao, K. P. C.; Harding, J. R.; Zhou, J.; Zuin, L.; Shao-Horn, Y. *Energy Environ. Sci.* **2011**, *4*, 2999−3007.
(31) Viswanathan, V.; Thygesen, K. S.; Hummelshoj, J. S.; Norskov, J. K.; Girishkumar, G.; McCloskey, B. D.; Luntz, A. C. *J. Chem. Phys.* **2011**, *135*, 214704.
(32) Radin, M. D.; Rodriguez, J. F.; Tian, F.; Siegel, D. J. *J. Am. Chem. Soc.* **2012**, *134*, 1093−1103.
(33) Gerbig, O.; Merkle, R.; Maier, J. *Adv. Mater.* **2013**, *25*, 3129−3133.
(34) Liu, Y.; Zheng, H.; Liu, X. H.; Huang, S.; Zhu, T.; Wang, J.; Kushima, A.; Hudak, N. S.; Huang, X.; Zhang, S.; Mao, S. X.; Qian, X.; Li, J.; Huang, J. Y. *ACS Nano* **2011**, *5*, 7245−7253.
(35) Yilmaz, E.; Yogi, C.; Yamanaka, K.; Ohta, T.; Byon, H. R. *Nano Lett.* **2013**, *13*, 4679−4684.
(36) McCloskey, B. D.; Speidel, A.; Scheffler, R.; Miller, D. C.; Viswanathan, V.; Hummelshøj, J. S.; Nørskov, J. K.; Luntz, A. C. *J. Phys. Chem. Lett.* **2012**, *3*, 997−1001.
(37) Itkis, D. M.; Semenenko, D. A.; Kataev, E. Y.; Belova, A. I.; Neudachina, V. S.; Sirotina, A. P.; Hävecker, M.; Teschner, D.; Knop-Gericke, A.; Dudin, P.; Barinov, A.; Goodilin, E. A.; Shao-Horn, Y.; Yashina, L. V. *Nano Lett.* **2013**, *13*, 4697−4701.
(38) Gallant, B. M.; Mitchell, R. R.; Kwabi, D. G.; Zhou, J.; Zuin, L.; Thompson, C. V.; Shao-Horn, Y. *J. Phys. Chem. C* **2012**, *116*, 20800−20805.
(39) Gu, M.; Parent, L. R.; Mehdi, B. L.; Unocic, R. R.; McDowell, M. T.; Sacci, R. L.; Xu, W.; Connell, J. G.; Xu, P.; Abellan, P.; Chen, X.; Zhang, Y.; Perea, D. E.; Evans, J. E.; Lauhon, L. J.; Zhang, J. G.; Liu, J.; Browning, N. D.; Cui, Y.; Arslan, I.; Wang, C. M. *Nano Lett.* **2013**, *13*, 6106−6112.